Depth-resolved approach for the attenuation coefficient calculation from the Optical Coherence Tomography data and its application for the brain imaging

Alexander Moiseev[*1], Ksenia Achkasova[2], Konstantin Yashin[2], Elena Kiseleva[2], Eugenia Bederina[2], Sergey Kuznetsov[2], Grigory Gelikonov[1], Pavel Shilyagin[1], Igor Medyanik[2], Elena Zagaynova[2,3] and Natalia Gladkova[2]

[1]Institute of Applied Physics, Russian Academy of Sciences, Ulyanova Str., 46, Nizhny Novgorod, Russia, 603950
[2]Privolzhsky Research Medical University, Minin sq., 10/1, Nizhny Novgorod, Russia, 603950
[3]Lobachevsky State University of Nizhny Novgorod, Gagarin av., 23, Nizhny Novgorod, Russia, 603950

ABSTRACT

Optical coherence tomography (OCT) is a promising tool for intraoperative tissue morphology determination. Several studies suggest that the attenuation coefficient, derived from the OCT images can differentiate between normal and tumorous tissues, as well as between gray and white brain matter. The methods used for attenuation coefficient derivation in these studies follow the assumption that the optical properties of the specimen are uniform within the OCT imaging depth range. Although this approximation is appropriate for the brain tissue, it is still quite restrictive. In the present study depth-resolved method for attenuation coefficient calculation was adopted for the real-world situation of the depth-dependent OCT sensitivity and additive imaging noise and applied to the imaging of the cadaveric brain. It was shown that the application of the less restrictive method for the attenuation calculation may reveal additional brain structures in the same dataset, as well as provide a statistically significant difference for the white matter attenuation coefficient in the different brain areas.

Keywords: cross-polarization OCT (CP OCT), attenuation coefficient, myelin fiber orientation, eloquent brain areas, image processing.

***Alexander Moiseev**, E-mail: alexander.moiseev@gmail.com, Phone: +79308000038

Introduction

Optical coherence tomography (OCT) is one of the most promising, innovative and rapidly emerging intraoperative imaging modalities for neurosurgical guidance during brain tumor surgery [1]. OCT can provide differentiation between tumorous and non-tumorous tissues through both qualitative [2-4] and quantitative assessment [5-7] of the OCT signal through optical properties calculation. Color-coded maps of optical coefficients can provide neurosurgeons with real-time high-resolution images clarifying the boundaries of the infiltrative brain tumors within surrounding tissues. Since the attenuation coefficient is the most frequently used optical property that can be estimated from the OCT data, it will be the primary focus of the present study.

Since several approaches exist for the attenuation coefficient calculation, the choice of the particular one may affect the outcome in terms of the method ability to differentiate between different types of brain tissue.

Assuming that the brain tissue is optically uniform within the OCT imaging depth range and applying Lambert-Beer law for the OCT signal intensity depth dependence, one can fit the OCT

signal intensity depth profile (A-scan) with the corresponding exponent to extract the signal attenuation [8]. More commonly however the logarithm of the OCT A-scan is linearly fitted [9-11], since such an approach does not require more computationally exhausting non-linear fitting. Recently proposed Fourier Domain calculation method proved to be more robust than the linear fitting approach, while maintaining its computational effectiveness [12].

All of the aforementioned methods imply the uniformity of the tissue optical properties within the imaging depth range and may lead to the erroneous results if this is not the case. In the present work the depth-resolved attenuation coefficient calculated method, proposed in [13], was adopted to the real-life situation of the depth-dependent OCT system sensitivity and the presence of the additive noise. The method works under the assumption that the backscattering coefficient is proportional to the attenuation coefficient and the proportionality coefficient is uniform in the OCT imaging depth range. While this is also a restrictive assumption, one should note that the tissue optical uniformity is its special case, since the optical uniformity within the range implies the uniformity of the backscattering/attenuation relation.

The adopted method was applied to the cadaveric brain specimen. It was shown that the application of the less restrictive method for the attenuation calculation may reveal additional brain structures in the same dataset, as well as provide statistically significant difference for the white matter attenuation coefficient in the different brain areas.

Results

Coefficient calculation methods comparison

The effect of the depth-resolved calculation on the maps of the attenuation coefficient distribution in the human brain can be seen in figure 1. One can see the maps of the attenuation coefficient distribution in the cadaveric human striatum calculated in different depth ranges from the OCT data with log-and-linear-fit approach (panels 1a,c,e,g) and the proposed depth-resolved approach (panels 1b,d,f,h). Firstly, the utilization of the log-and fit approach in the smaller depth range of 60 μm (20 pixels in the OCT data volume) leads to the low SNR of the resulting images (panels 1a,c,e) with the details of the image completely obfuscated by the noise. To overcome this drawback and reveal fine details in the attenuation coefficient distribution with the log-and-linear-fit method, larger depth range should be utilized (in the panel g the map for the depth range of 180 μm (60 pixels) is presented). Secondly, the utilization of the depth-resolved method leads to the images with higher SNR and reveals fine details in the images, calculated in the smaller 60 μm depth range (panes 1b,d,f). Thirdly, images in the panes 1b,d,f reveal the

evolution of the map with the depth, which implies that the underlying assumption for the log-and-linear-fit method does not hold for this specimen of the human brain.

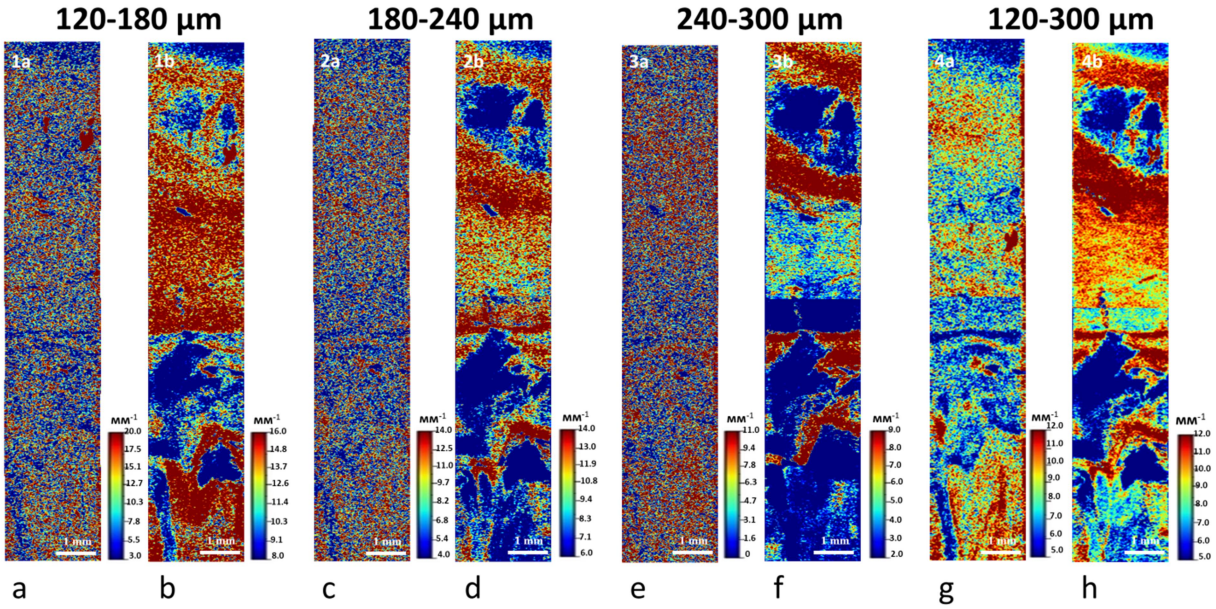

Figure 1. Attenuation coefficient distribution maps in the cadaveric human striatum. **a,c,e,g** – distributions calculated from the OCT data with log-and-linear-fit method in the depth range 120-180 µm, 180-240 µm, 240-300 µm and 120-300 µm respectively. **b,d,f,h** – distributions calculated from the OCT data with the proposed depth-resolved method in the depth range 120-180 µm, 180-240 µm, 240-300 µm and 120-300 µm respectively.

In the figure 2 one can see the comparison of the attenuation coefficient distribution maps calculated for the specimen of the cadaveric brain with two studied approaches in the depth range 180 µm (60 pixels). The utilization of the depth-resolved method of the attenuation coefficient calculation reveals fine details in the corresponding distributions (see panel 2c and corresponding close-ups 2c1,c2,c3,c4 in comparison with the panel 2b and close-ups 2b1,b2,b3,b4, calculated with the log-and-linear-fit method).

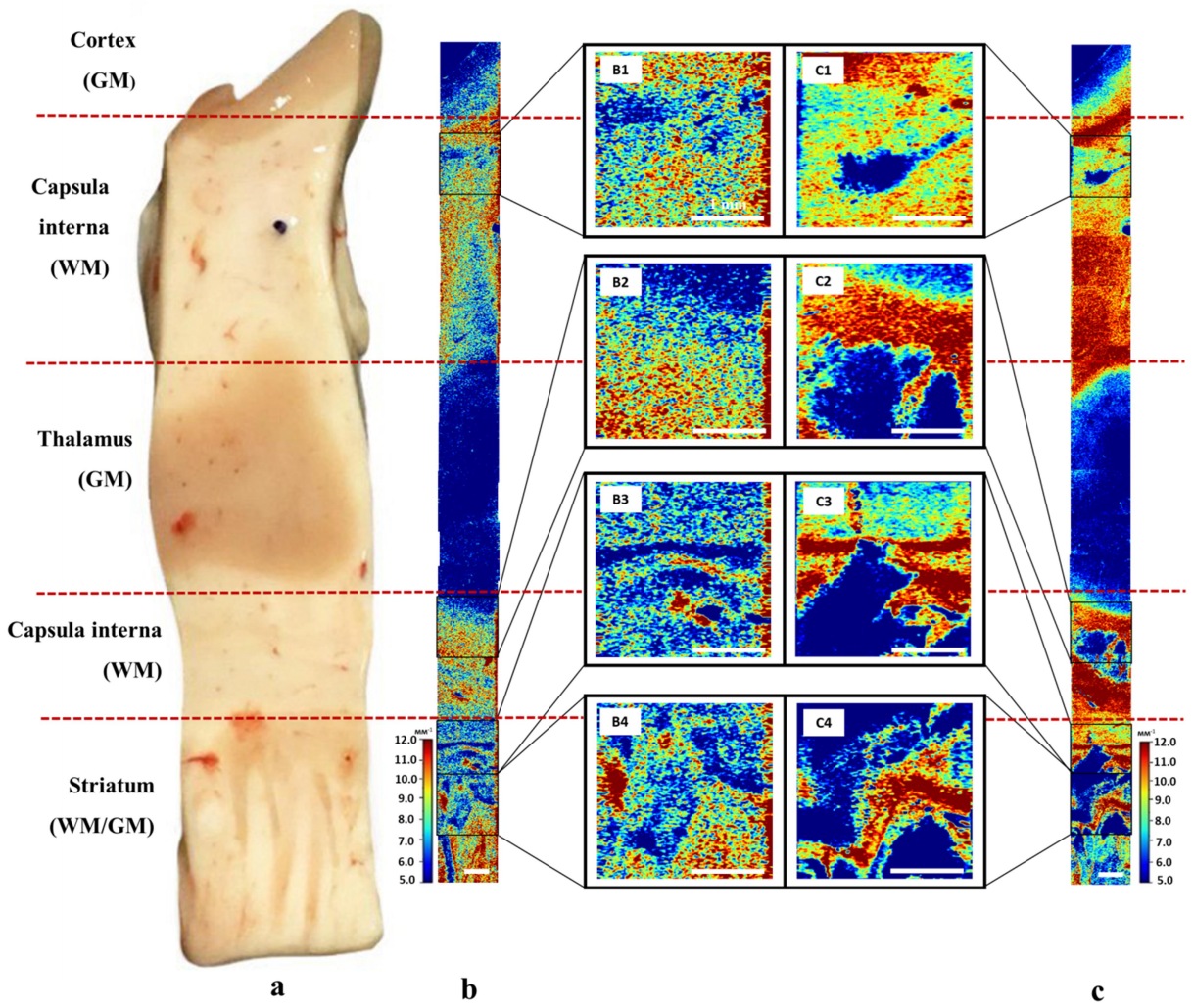

Figure 2. **a** – Photo of the cadaveric human brain specimen. **b** – attenuation coefficient distribution maps of the specimen calculated from the OCT data with log-and-linear-fit method in the depth range 120-300 µm. **c** – attenuation coefficient distribution maps of the specimen calculated from the OCT data with the proposed depth-resolved method in the depth range 120-300 µm. in the cadaveric human striatum. **b1-b4**, **c1-c4** – parts of the images in the panels b and c respectively magnified for convenient comparison.

Attenuation coefficient of the white matter from different brain areas

The utilization of the depth resolved coefficients reveals the statistically significant difference in the attenuation coefficient values for the white matter samples obtained from different brain structures. In Table 1 the values for attenuation coefficient of the brain samples taken from 5 different brain structures are presented (corpus callosum, U-shaped fibers, capsula interna, long-range fibers and brain stem).

	U-shaped fibers (n=14)	Long-Range Association Fibers (n=22)	Capsula Interna (n=10)	Corpus Callosum (n=8)	Brainstem (n=11)
log-and-linear-fit method	8,55	8,80	7,86	8,08	9,20
depth-resolved method	10,78	9,53	8,52	8,98	8,45

Table 1. Median, 25th and 75th percentiles values for attenuation coefficient of the brain samples taken from 5 different brain .

In Tables 2 and 3 the result of the pairwise comparison of the distribution of the attenuation coefficient in the corresponding structures using the Mann-Whitney test are presented. The utilization of the log-and-linear-fit does not allow differentiating the structures with statistical significance (see Table 2). At the same time, proposed depth-resolved approach makes it possible (see Table 3). One can see that the values of the attenuation coefficient of the U-shaped fibers are higher (with statistical significance higher than 0.05) than the values in all other structures, while the values of the attenuation coefficient of the brain stem are statistically lower (with statistical significance higher than 0.05) than the values in all other structures except the capsula interna.

	Corpus callosum	U-shaped fibers	Capsula interna	Long range fibers	Brain stem
Corpus callosum		0.57	0.057	0.40	0.74
U-shaped fibers	0.44		0.052	0.43	0.75
Capsula interna	0.95	0.95		0.93	0.94
Long range fibers	0.61	0.58	0.07		0.69
Brain stem	0.27	0.26	0.06	0.31	

Table 2. P-values for the one-tailed Mann-Whitney test with the alternative hypothesis that the values for the attenuation coefficient distributions in the brain areas in the rows are bigger than the values in the columns. The attenuation coefficients were calculated with the log-and-linear-fit method.

	Corpus	U-shaped	Capsula	Long range	Brain stem

	callosum	fibers	interna	fibers	
Corpus callosum		0.995	0.13	0.40	**0.017**
U-shaped fibers	**0.0058**		**0.0006**	**0.00044**	**0.000032**
Capsula interna	0.9	0.9994		0.9	0.19
Long range fibers	0.60	0.9996	0.10		**0.007**
Brain stem	0.98	0.9997	0.82	0.993	

Table 3. P-values for the one-tailed Mann-Whitney test with the alternative hypothesis that the values for the attenuation coefficient distributions in the brain areas in the rows are bigger than the values in the columns. The attenuation coefficients were calculated with the proposed depth-resolved method. The p-values below 0.05 are typed in the bold font.

Discussion

Although the depth-resolved approach for the attenuation coefficient calculation from the OCT data was derived in assumption of the constant proportionality between the attenuation and backscattering coefficients through the OCT imaging depth and the assumption was not thoroughly tested and thus might not hold in the real-world situation, it is still a generalization for the widely used method which implies samples optical uniformity through the OCT imaging depth. The utilization of such more general method has several advantages. Firstly, it allows attenuation coefficient calculations in smaller depth range, thus providing better axial resolution in comparison with the methods implying optical uniformity. Secondly, it reveals finely resolved details of the underlying structures, thus providing the user with higher amount of the relevant information. Thirdly, it is sensitive to the different types of the white matter, which potentially may allow white matter preservation state estimation, which, in turn may allow surgeon to make the decision about the resection borders.

The observed differences can be explained by the difference in the myelination rate in the corresponding white matter areas. White matter mainly consists of neuronal fibers (~60%) [1, 3]. The majority of the fibers are enveloped by a myelin sheath - myelinated fibers (70 to 95% of all nerve fibers) [2]. Regardless the white matter is highly hydrated (~72%) [4], while the myelin sheath is characterized by relatively low water content (~40%) [6, 14] and myelin presents 50 to 60% of the dry tissue weight [5]. Previous studies have demonstrated that the OCT signal reflects the level of water content in the brain and dehydrated tissue is characterized by high

attenuation of the OCT signal [7, 15]. Considering these facts, the myelin is seemed to be the main component affecting the attenuation of the OCT signal in the present study.

Although the potential of the proposed method has been demonstrated in the study, further development is needed for its clinical translation. Firstly, the myelination rate hypothesis should be tested on the bigger dataset with more subjects from diverse groups involved. Secondly, the myelination rate hypothesis should be verified in *in vivo* studies. Thirdly, the hypothesis should be verified by the independent method, i.e. systematical histology study. Thirdly, some improvements should be made to the OCT device, first of all to its resolution, since better resolution may provide better insights into the local neural fiber structures.

Conclusion

The depth-resolved approach for the attenuation coefficient calculation from the OCT data presents the differences between white matter of different brain areas. The detection of white matter density during surgery of infiltrative brain tumors looks promising but additional CP OCT performance build-up and resolution enhancement are needed. The main interest in brain tumor surgery will be to detect intraoperatively the direction of myelin fibers within surrounding white matter.

Methods

Tissue samples

The study was conducted on 8 fresh anatomical specimens (4 left and 4 right hemispheres) of the brain of adults aged 58 to 69 years, whose death was not caused by intracranial pathology.

The white matter specimens were obtained from following brain areas: (1) cortical - U-shaped fibers (n=14); (2) subcortical - long-range association fibers (n=22); (3) capsula interna (n=10); (4) corpus callosum (n=8); (5) brainstem (n=11).

All specimens were delivered to the location of the OCT study which took 10 minutes for each specimen. The study was approved by the Ethical Committee of the Privolzhsky Research Medical University, and informed consent was obtained from each subject`s legal guardian. All methods were performed in accordance with the relevant guidelines and regulations.

OCT study and image analysis

The study was performed with a spectral-domain OCT (SD OCT) device developed in the Institute of Applied Physics of the Russian Academy of Sciences (Nizhny Novgorod, Russia). The device has a 20,000 A-scan/s scanning rate and performs 2D lateral scanning with a range of 2.4 × 2.4 mm to obtain a 3D distribution of backscattered light in the polarization parallel and orthogonal to the polarization of the probing beam.

Depth-resolved attenuation coefficient

According to [13] depth-resolved attenuation coefficient can be calculated from the OCT data as follows:

$$\mu_i = \frac{I_i}{2\Delta\sum_{i+1}^{\infty} I_j} \quad (1)$$

Where I_i is the OCT signal intensity, i_{max} is the index of the maximal depth in the OCT image.

The method works under the two assumptions. Firstly, the backscattering coefficient is proportional to the attenuation coefficient and the proportionality coefficient is uniform in the OCT imaging depth range. Secondly, the light is completely attenuated within the OCT imaging depth range, i.e. the intensity integral from some depth in the OCT image to the infinity is equal to the intensity integral from this depth to the maximal OCT imaging depth.

If the Equation (1) is applied directly to the experimentally measured OCT signal, the following estimation can be obtained:

$$\mu_i^{est} = \frac{A_i \cdot I_i + N_i}{2\Delta\sum_{i+1}^{i_{max}}\left[A_j \cdot I_j + N_j\right]} = \frac{A_i \cdot I_i + N_i}{2\Delta\sum_{i+1}^{\infty} A_j \cdot I_j - 2\Delta\sum_{i_{max}}^{\infty} A_j \cdot I_j + 2\Delta\sum_{i+1}^{i_{max}} N_j} = \frac{A_i \cdot I_i + N_i}{2\Delta\left[\sum_{i+1}^{\infty} A_j \cdot I_j + \sum_{i+1}^{i_{max}} N_j\right]} \quad (2)$$

Where A_i is the multiplier accounts for the depth-dependent sensitivity of the OCT system, N_i is the additive noise. In a SD OCT device depth-dependent sensitivity arises due to the confocality of the optical system and the sensitivity roll-off due to the finite size of the spectrometer elements [8, 16]. The noise has nonzero mean due to the absolute value and square operations taken to convert complex OCT signal to the OCT signal intensity.

The difference between sought-for estimate (1) and the estimate from the actual signal (2) can be written as:

$$\mu_i - \mu_i^{est} = \mu_i - \frac{A_i \cdot I_i + N_i}{2\Delta\left[\sum_{i+1}^{\infty} A_j \cdot I_j - \sum_{i+1}^{i_{\max}} N_j\right]} =$$

$$\frac{\mu_i \cdot 2\Delta \cdot \sum_{i+1}^{\infty} A_j \cdot I_j - \mu_i \cdot 2\Delta \cdot \sum_{i+1}^{i_{\max}} N_j - A_i \cdot I_i \cdot \frac{2\Delta \cdot \sum_{i+1}^{\infty} I_j}{2\Delta \cdot \sum_{i+1}^{\infty} I_j} - N_i}{2\Delta\left[\sum_{i+1}^{\infty} A_j \cdot I_j - \sum_{i+1}^{i_{\max}} N_j\right]} =$$

$$\frac{\mu_i \cdot 2\Delta \cdot \sum_{i+1}^{\infty} A_j \cdot I_j - \mu_i \cdot 2\Delta \cdot \sum_{i+1}^{i_{\max}} N_j - A_i \cdot \mu_i \cdot 2\Delta \cdot \sum_{i+1}^{\infty} I_j - N_i}{2\Delta\left[\sum_{i+1}^{\infty} A_j \cdot I_j - \sum_{i+1}^{i_{\max}} N_j\right]} =$$

$$\frac{\mu_i \cdot \left[\sum_{i+1}^{\infty} A_j \cdot I_j - A_i \sum_{i+1}^{\infty} I_j - \sum_{i+1}^{i_{\max}} N_j\right]}{\sum_{i+1}^{\infty} A_j \cdot I_j - \sum_{i+1}^{i_{\max}} N_j} - \frac{N_i}{2\Delta\left[\sum_{i+1}^{\infty} A_j \cdot I_j - \sum_{i+1}^{i_{\max}} N_j\right]} \quad (3)$$

Thus the relation between (2) and (1) can be rewritten as:

$$\mu_i^{est} = \mu_i \cdot \left[1 - \frac{\sum_{i+1}^{\infty} A_j \cdot I_j - A_i \sum_{i+1}^{\infty} I_j - \sum_{i+1}^{i_{\max}} N_j}{\sum_{i+1}^{\infty} A_j \cdot I_j - \sum_{i+1}^{i_{\max}} N_j}\right] + \frac{N_i}{2\Delta\left[\sum_{i+1}^{\infty} A_j \cdot I_j - \sum_{i+1}^{i_{\max}} N_j\right]}$$

$$\mu_i^{est} = \mu_i \cdot \left[\frac{A_i \sum_{i+1}^{\infty} I_j}{\sum_{i+1}^{\infty} A_j \cdot I_j - \sum_{i+1}^{i_{\max}} N_j}\right] + \frac{N_i}{2\Delta\left[\sum_{i+1}^{\infty} A_j \cdot I_j - \sum_{i+1}^{i_{\max}} N_j\right]} \quad (4)$$

To obtain a robust estimation of the (1) having the (2) one should account for signal-to-noise ratio (SNR) within the image. In the regions with low SNR simple division will lead to the noise amplification. Such an estimation can be done with the Wiener-type approach:

$$\mu_i = \frac{H_i \cdot SNR_i}{|H_i|^2 \cdot SNR_i + 1} \cdot \mu_i^{est}$$

$$H_i = \frac{A_i \sum_{i+1}^{\infty} I_j}{\sum_{i+1}^{\infty} A_j \cdot I_j - \sum_{i+1}^{i_{\max}} N_j} \approx \frac{A_i \sum_{i+1}^{i_{\max}} I_j^{est}}{\sum_{i+1}^{i_{\max}} A_j \cdot I_j - \sum_{i+1}^{i_{\max}} N_j}$$

$$SNR_i = \sum_{x_i, z_i \in W} \frac{|\mu_i^{est}|^2 - |N_i^{\mu}|^2}{|N_i^{\mu}|^2}$$

$$N_i^{\mu} = \frac{N_i}{2\Delta\left[\sum_{i+1}^{\infty} I_j + \sum_{i+1}^{i_{\max}} N_j\right]} = \frac{\langle N \rangle}{2\Delta\left[\sum_{i+1}^{i_{\max}} I_j + \sum_{i+1}^{i_{\max}} N_j\right]} \quad (5)$$

Where I^{est} is the true signal estimate that should be made from the measurement, <N> is the mean noise. One should note that the integrals in the denominators in (5) could be calculated directly from the OCT data. The signal estimates I^{est} can be made by finding the least-squares solution of the following system of linear equations:

$$\sum_{i+1}^{i_{\max}} A_j \cdot I_j^{est} = \left[\sum_{i+1}^{i_{\max}} A_j \cdot I_j - \sum_{i+1}^{i_{\max}} N_j\right] - \sum_{i+1}^{i_{\max}} \langle N \rangle \quad (6)$$

One should also note that in the case of the uniform OCT system sensitivity the H_i term in (5) can be rewritten as [17]:

$$H_i = 1 - \frac{\sum_{i+1}^{\infty} N_j}{\sum_{i+1}^{\infty} I_j + \sum_{i+1}^{i_{\max}} N_j} = 1 - \frac{\langle N \rangle \cdot (i_{max} - i)}{\sum_{i+1}^{i_{\max}} I_j + \sum_{i+1}^{i_{\max}} N_j} \quad (7)$$

To reduce the speckle influence on the results, the experimental OCT data volumes were convolved in 3D with 3x3x3 window before the application of the method.

Log-and-linear-fit attenuation coefficient estimation

Considering brain tissue is optically homogeneous, the OCT signal depends exponentially on depth:

$$I_i \sim \exp(-2\mu z_i) \quad (8),$$

where I_i is the OCT signal, μ is the specimen attenuation coefficient, z_i is the depth coordinate. Taking the logarithm of the OCT signal depth dependency makes it linear from the depth. Thus, linear fitting of the logarithm of the signal allows one obtaining the attenuation coefficient in assumption of its uniformity over the OCT imaging depth.

To reduce the speckle influence on the results, the experimental OCT data volumes were convolved in 3D with 3x3x3 window before the application of the method.

Histological study

Brain samples were fixed in 10% formalin for 48 hours and a series of histological sections was made. The histological sections were stained with hematoxylin and eosin (H&E) and Luxol fast blue stain with crezyl violet (to identify both myelinated fibers and the neuronal tissue structures).

Statistical analysis

The mode value (the most probable value) was extracted for each of the obtained sample maps of attenuation coefficient distributions as a value where histogram with 256 bins reaches its maximum. Such a characteristic was chosen because some samples have bimodal distributions due to the presence of the gray matter and other more conventional characteristics such as mean and median gave the biased result. The distributions of the obtained mode values of all attenuation coefficient maps for each of the brain area were used for further statistical analysis. The mean values of such distributions are presented in the Table 1. To distinguish tissue types by each coefficient, we used the Mann-Whitney U-test with the hypothesis that there was no difference between the compared groups. The results of such comparison are presented in the Tables 2 and 3.

Acknowledgments

Development of an approach for quantitative assessment of CP OCT data was supported by the Russian Foundation for Basic Research, grant No 18-29-01049. The OCT device development was supported by the State Task of IAP RAS No 0035-2019-0013.

References

1. Mottershead, J., et al., *High field MRI correlates of myelin content and axonal density in multiple sclerosis.* Journal of neurology, 2003. **250**(11): p. 1293-1301.
2. Liewald, D., et al., *Distribution of axon diameters in cortical white matter: an electron-microscopic study on three human brains and a macaque.* Biological cybernetics, 2014. **108**(5): p. 541-557.
3. Stikov, N., et al., *Quantitative analysis of the myelin g-ratio from electron microscopy images of the macaque corpus callosum.* Data in brief, 2015. **4**: p. 368-373.
4. Tofts, P., *Quantitative MRI of the brain: measuring changes caused by disease*2005: John Wiley & Sons.

5. Norton, W.T. and L.A. Autilio, *The lipid composition of purified bovine brain myelin.* Journal of neurochemistry, 1966. **13**(4): p. 213-222.
6. Norton, W.T. and W. Cammer, *Isolation and characterization of myelin*, in *Myelin*1984, Springer. p. 147-195.
7. Rodriguez, C.L., et al., *Decreased light attenuation in cerebral cortex during cerebral edema detected using optical coherence tomography.* Neurophotonics, 2014. **1**(2): p. 025004.
8. Faber, D.J., et al., *Quantitative measurement of attenuation coefficients of weakly scattering media using optical coherence tomography.* Optics express, 2004. **12**(19): p. 4353-4365.
9. Kut, C., et al., *Detection of human brain cancer infiltration ex vivo and in vivo using quantitative optical coherence tomography.* Science translational medicine, 2015. **7**(292): p. 292ra100-292ra100.
10. Tomlins, P.H., et al., *Scattering attenuation microscopy of oral epithelial dysplasia.* Journal of biomedical optics, 2010. **15**(6): p. 066003.
11. Yashin, K.S., et al., *Quantitative nontumorous and tumorous human brain tissue assessment using microstructural co-and cross-polarized optical coherence tomography.* Scientific reports, 2019. **9**(1): p. 1-12.
12. Yuan, W., et al., *Robust and fast characterization of OCT-based optical attenuation using a novel frequency-domain algorithm for brain cancer detection.* Scientific reports, 2017. **7**: p. 44909.
13. Vermeer, K., et al., *Depth-resolved model-based reconstruction of attenuation coefficients in optical coherence tomography.* Biomedical optics express, 2014. **5**(1): p. 322-337.
14. Morell, P., R.H. Quarles, and W. Norton, *Myelin formation, structure and biochemistry.* Basic neurochemistry, 1999: p. 117-143.
15. Kiseleva, E., et al., *Cross-Polarization Optical Coherent Tomography in Comparative in vivo and ex vivo Studies of Optical Properties of Normal and Tumorous Brain Tissues.* Sovrem. Tehnol. Med, 2017. **9**(4 (eng)).
16. Hagen-Eggert, M., P. Koch, and G. Hüttmann. *Analysis of the signal fall-off in spectral domain optical coherence tomography systems*. in *Optical Coherence Tomography and Coherence Domain Optical Methods in Biomedicine XVI*. 2012. International Society for Optics and Photonics.
17. Gubarkova, E.V., et al., *Tissue optical properties estimation from cross-polarization OCT data for breast cancer margin assessment.* Laser Physics Letters, 2020. **17**(7): p. 075602.